Origin of chaos in 3-d Bohmian trajectories

Athanasios C. Tzemos, George Contopoulos, Christos Efthymiopoulos

Research Center for Astronomy and Applied Mathematics of the Academy of Athens, Soranou Efesiou 4, GR-11527 Athens, Greece

arXiv:1609.07069v1 [quant-ph] 22 Sep 2016

Abstract

We study the 3-d Bohmian trajectories of a quantum system of three harmonic oscillators. We focus on the mechanism responsible for the generation of chaotic trajectories. We demonstrate the existence of a 3-d analogue of the mechanism found in earlier studies of 2-d systems [1, 2], based on moving 2-d 'nodal point - X-point complexes'. In the 3-d case, we observe a foliation of nodal point - X-point complexes, forming a '3-d structure of nodal and X-points'. Chaos is generated when the Bohmian trajectories are scattered at one or more close encounters with such a structure.

Keywords: Bohmian Quantum Mechanics, Chaos

1. Introduction

The Bohmian picture of quantum mechanics [3, 4] has attracted the attention of many researchers in the last two decades, due not only to its potential theoretical interest [5, 6], but also to its wide spectrum of applications in the fields of atomic and molecular physics, nanoelectronics, light-matter interaction etc (see [7, 8]). In the Bohmian picture, besides the evolution of the particle wavefunction, governed by the Schrödinger equation

$$\Big[-\frac{\hbar^2}{2m}\nabla^2 + V \Big]\Psi(\vec{x},t) = i\hbar\frac{\partial\Psi(\vec{x},t)}{\partial t}, \tag{1}$$

we consider also particle trajectories governed by the 'guidance' equation

$$m\frac{d\vec{x}}{dt} = \hbar\Im\Big(\frac{\nabla\Psi(\vec{x},t)}{\Psi(\vec{x},t)}\Big). \tag{2}$$

In the Bohmian interpretation, these trajectories acquire 'ontological' significance as part of the physical reality of microscopic systems. However, the Bohmian trajectories can also be viewed as tracers of the quantum probability flow, a fact allowing to regard the Bohmian picture as a trajectory-based approach for studying the time evolution of quantum processes also in the framework of the conventional interpretation of quantum mechanics (see [9]).

An important topic in Bohmian mechanics is the emergence of *chaos* and the role played by chaotic Bohmian trajectories. It has been suggested that Bohmian chaos is relevant in the interpretation of a variety of quantum phemomena. Examples are: i) the precision limits of hydrodynamical solvers of Schrödinger's equation (e.g. [8, 10, 11]), and ii) 'quantum relaxation', i.e., the possibility to assign a dynamical origin to Born's rule for the quantum probabilities [12]. More examples are dicussed in [7].

The mechanism of generation of chaos is thought to be well understood in 2-d quantum systems [1, 2, 13, 14, 15, 16, 17, 18, 19, 20, 21]. However, only few works exist in the 3-d or higher dimensional cases, due to the far higher complexity of the problem [16, 22, 23, 24].

In this letter we study an example of 3-d quantum system, aiming to investigate the origin of chaos and the dynamical properties of 3-d chaotic Bohmian trajectories.

The Hamiltonian consists of three harmonic oscillators

$$H = \sum_{k=1}^{3}\Big(\frac{p_k^2}{2m} + \frac{1}{2}m_k\omega_k^2 x_k^2\Big). \tag{3}$$

As exemplified in section 2 below, the quantum states of the system (3) typically exhibit both regular and chaotic Bohmian trajectories. Focusing on the latter, in our study below we extend the results found in corresponding 2-d cases, which in summary are the following:

1. In the vicinity of the nodal points (i.e. the points in configuration space where the wavefunction becomes null $\Psi = 0$) we observe, in general, the formation of quantum vortices. A vortex around a nodal point is visualized by drawing the 2-d vector field of the probability flow in a system of reference co-moving with the nodal point.

2. Near every nodal point, we can prove the existence of a second critical point of the flow in the comoving frame. This second point is always hyperbolic, and it was called the X-point in refs. [1, 2]. The chaotic behavior of the trajectories is due to the cumulative effect of their repeated close encounters with the X-points (while, as noted already in [3, 4], the trajectories avoid, in general, coming close to the corresponding moving nodal points). In particular, the 'stretching number' (i.e. the local Lyapunov exponent) of a trajectory undegoes a positive kick at every such close

*A.C. Tzemos , Tel: +306932271598

Email addresses: thanasistzemos@gmail.com (Athanasios C. Tzemos), gcontop@academyofathens.gr (George Contopoulos), cefthim@academyofathens.gr (Christos Efthymiopoulos)

encounter. The above mechanism of chaos is generic for 2-d systems, in the sense that its existence is guaranteed by a local analysis of the quantum flow near every nodal point generated by an arbitrary 2-d wavefunction [2].

3. The 2-d structure formed by a nodal point and its associated X-point, as well as the latter's stable and unstable manifolds and all nearby streamlines of the quantum probability flow, is called a 'nodal point - X-point complex'. A demonstrated in [2], the nodal point-X-point structure of the quantum flow is generic close to *moving* nodal points, i.e. this structure necessarily appears in the frame of reference comoving with any nodal point. On the other hand, we may have different topologies appearing close to fixed nodal points, which however, cannot lead to chaos.

In the present letter, we show that these results can be extended to the 3-d case.

An important early work in the 3-d case was provided by Falsaperla and Fonte [23], who made a careful analysis of the quantum flow, based on a leading order expansion of the Bohmian equations of motion around nodal points. These authors found that: i) the streamlines of the quantum flow lie locally on planes orthogonal to a "nodal line", i.e. a line formed in the 3-d configuration space by continuously joining the nodal points of the solutions of $\Psi = 0$ for a given time. ii) The local form of the streamlines is spiral and the union of all these spirals surrounds the nodal line forming a "cylindrical structure". This structure influences the form of the trajectories close to nodal lines. However, according to [23], the dynamical behavior of the trajectories close to the nodal points appears "regular", while chaos is attributed to an "intermittent" "switch back and forth" from the vicinity of one nodal line to that of another nodal line.

Here we demonstrate that, similarly to the 2-d case, in each of the orthogonal planes discussed already in [23], the structure of the quantum flow is such as to form, besides the nodal point, also an X-point, and hence, a complete 2-d nodal point X-point complex. We compute numerically several such complexes for various times and in various locations of the 3-d configuration space and establish that their topological structure is similar to those established in the 2-d case. However, in the 3-d case, the ensemble of all the orthogonal planes forms a foliation. Then, besides joining the nodal points along this foliation, thus forming a 'nodal line', we can also join the X-points, thus forming an 'X-line'. The whole geometrical structure of the quantum flow formed in this way is hereafter called a '3-d structure of nodal and X-points'. This structure extends the "cylindrical structure" observed in [23], by adding the X-points to it. This extension is crucial for understanding the generation of chaos. Namely, chaos is produced by the repeated scatterings of the Bohmian trajectories with the X-points along the 3-d structure of nodal and X-points. In fact, this mechanism implies that chaotic trajectories in 3-d systems can exist even when only one such structure is present for every time, i.e., one does not need the intermittent jumps between more than one such structure, that were conjectured in [23]. On the other hand, we leave open the question of how general our presently proposed chaos mechanism is.

In section 2, we consider a basic 3-d quantum state of the Hamiltonian (3) in which the orthogonal relation between the quantum flow and the nodal lines is exact. This model serves to establish the basic features of the chaos mechanism and to show the '3-d structure of nodal and X-points'. Yet, this model is not generic since Bohmian trajectories cannot exhibit any motion in the direction normal to the orthogonal planes, i.e. along the 3-d structure of nodal and X-points. However, in section 3 we perturb our previous state in a way so as to secure the occurrence of genuinely 3-d chaotic diffusion. Finally, section 4 summarizes the conclusions of our present study.

2. Basic Model

Equations of motion: In the Hamiltonian (3) we studied the Bohmian trajectories in several cases of wavefunctions of the form

$$\Psi(\vec{x},t)=\sum_{i=1}^{3}a_i e^{-\frac{i}{\hbar}E_i t}\Psi_i(\vec{x}),\quad \sum_{i=1}^{3}|a_i|^2=1 \tag{4}$$

where $\Psi_i(\vec{x}), i=1..3$ are eigenstates of the form

$$\Psi(\vec{x})=\prod_{k=1}^{3}\frac{\left(\frac{m_k\omega_k}{\hbar\pi}\right)^{\frac{1}{4}}\exp\left(\frac{-m_k\omega_k x_k^2}{2\hbar}\right)}{\sqrt{2^{n_k}n_k!}}H_{n_k}\Big(\sqrt{\frac{m_k\omega_k}{\hbar}}x_k\Big), \tag{5}$$

where m_k are the masses, ω_k the frequencies of the oscillators and H_{n_k} are the Hermite polynomials of order n_k. The energy of the eigenstate (5) is $E=\sum_{k=1}^{3}(n_k+\frac{1}{2})\hbar\omega_k$. We work in units in which $m_1=m_2=m_3=\hbar=1$, while we set $\omega_1=1,\omega_2=\sqrt{2},\omega_3=\sqrt{3}$.

We computed trajectories in several examples of wavefunctions of the form (4), and we typically found both ordered and chaotic Bohmian trajectories. In the sequel, we focus on one particular of these examples, namely

$$\Psi(\vec{x},t)=\frac{\Psi_{1,0,0}(\vec{x},t)+\Psi_{0,1,0}(\vec{x},t)+\Psi_{0,0,1}(\vec{x},t)}{\sqrt{3}}. \tag{6}$$

The wavefunction (6) turns to be convenient in our analysis below due to the following property: The Bohmian equations of motion, derived from Eq.(2) are:

$$\dot{x_i}=\frac{1}{G}\sum_{\substack{j=1\\ i\neq j}}^{3}\sqrt{(\omega_j\omega_i)}\sin(\omega_{ji}t)x_j, \tag{7}$$

where $G=\sum_{i=1}^{3}\left(\sum_{\substack{j=1\\ j\neq i}}^{3}\left(\sqrt{\omega_i\omega_j}\cos(\omega_{ij}t)x_ix_j+\omega_i^2x_i^2\right)\right)$ and $\omega_{ij}=\omega_i-\omega_j$.

From Eqs. (7) we derive that $\sum_{i=1}^{3} x_i \dot{x}_i = 0$. Therefore all the Bohmian trajectories lie on spherical surfaces

$$\sum_{i=1}^{3} x_i^2 = R^2 \tag{8}$$

with R determined from the initial conditions.

Nodal point-X-point complexes: The nodal points are the solutions, for (x_1, x_2, x_3), of the system of equations

$$Re(\Psi(x_1, x_2, x_3, t)) = 0, \quad Im(\Psi(x_1, x_2, x_3, t)) = 0. \tag{9}$$

Since (9) is a system of 2 equations for 3 variables, the solutions lie, in general, along curves in the 3-d space. In our particular case any solution $x_1 = x_{1nod}, x_2 = x_{2nod}, x_3 = x_{3nod}$ of (9) satisfies the relation

$$\frac{\sqrt{\omega_1} x_{1nod}}{\sin(\omega_{32} t)} = \frac{\sqrt{\omega_2} x_{2nod}}{\sin(\omega_{13} t)} = \frac{\sqrt{\omega_3} x_{3nod}}{\sin(\omega_{21} t)} = C. \tag{10}$$

Consequently the nodal points all lie along straight lines in 3-d space passing through the origin $(0, 0, 0)$, whose inclination changes with the time t.

Consider, now, the intersection of such a line with the surface of the sphere of fixed radius R. The point of intersection is a nodal point describing a trajectory on the sphere. Due to Eq.(10) we have $\sqrt{\omega_2\omega_3}\sin(\omega_{32}t)\dot{x}_{1nod} + \sqrt{\omega_1\omega_3}\sin(\omega_{13}t)\dot{x}_{2nod} + \sqrt{\omega_1\omega_2}\sin(\omega_{21}t)\dot{x}_{3nod} = 0$. Thus, the velocity of the nodal point is perpendicular to the corresponding nodal line. Figure 1a shows the trajectory of the nodal point on the surface $R = 4.23$ from $t = 1$ (blue point) up to $t = 250$. This trajectory passes several times through some convergence points, near which the velocity and acceleration of the nodal point increases considerably (Fig. 1b).

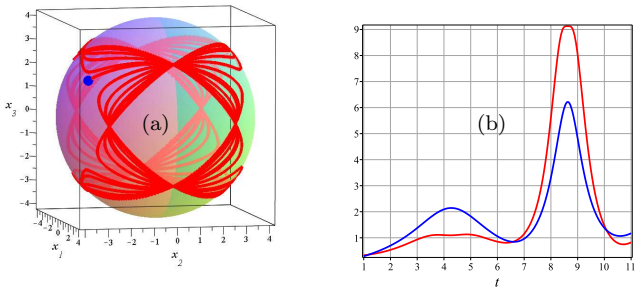

Figure 1: (a) The trajectory of a nodal point starting at a distance 4.23 from (0,0,0) for $t = 1$ (blue point) up to $t = 250$. This trajectory is on the surface of a sphere (strong red lines on the foreground and weaker lines on the background of the sphere). (b) The velocity (blue curve) and the acceleration (red curve) of a nodal point as functions of time. Both increase abruptly near a convergence point at $t \simeq 8.5$.

We will now examine the structure of the quantum flow in a moving plane tangent to the sphere of fixed radius R (like the one of Fig. 1a), at a point coinciding with the instantaneous position of the nodal point on the same sphere at any time t (this plane coincides with the plane 'orthogonal to the nodal line' defined in [23]). To this end, we define a non-inertial frame of reference (x_1', x_2', x_3') whose x_3'-axis coincides, at any time t, with the corresponding nodal line of Eq. (10). The change of coordinates $(x_1, x_2, x_3) \rightarrow (x_1', x_2', x_3')$ is realized via the transformation

$$\vec{x'} = S\vec{x}, \quad \dot{\vec{x}}' = S\dot{\vec{x}}, \tag{11}$$

where $S(t) = \begin{pmatrix} \sin\phi(t) & -\cos\phi(t) & 0 \\ \cos\theta(t)\cos\phi(t) & \cos\theta(t)\sin\phi(t) & -\sin\theta(t) \\ \sin\theta(t)\cos\phi(t) & \sin\theta(t)\sin\phi(t) & \cos\theta(t) \end{pmatrix}$, with $\cos\theta(t) = \frac{x_{3nod}(t;R)}{\sqrt{\sum_{i=1}^{3} x_{inod}(t;R)^2}}$ and $\tan\phi(t) = \frac{x_{2nod}(t;R)}{x_{1nod}(t;R)}$, $\theta \in [0, \pi]$ and $\phi \in [0, 2\pi)$. Setting $\vec{U} = (u, v, w)$, where $u = x_1 - x_{1nod}(t), v = x_2 - x_{2nod}(t), w = x_3 - x_{3nod}(t)$, $A(t) = \begin{pmatrix} 0 & -\sqrt{\omega_1\omega_2}\sin(\omega_{12}t) & -\sqrt{\omega_1\omega_3}\sin(\omega_{13}t) \\ \sqrt{\omega_1\omega_2}\sin(\omega_{12}t) & 0 & -\sqrt{\omega_2\omega_3}\sin(\omega_{23}t) \\ \sqrt{\omega_1\omega_3}\sin(\omega_{13}t) & \sqrt{\omega_2\omega_3}\sin(\omega_{23}t) & 0 \end{pmatrix}$ and using (10), Eqs. (7) take the form

$$\dot{\vec{U}}' = S(t)\dot{\vec{U}} = \frac{1}{G}S(t)A(t)S^{-1}(t)\vec{U}' - S(t)\dot{\vec{x}}_{nod}. \tag{12}$$

Consequently

$$\begin{pmatrix} \dot{u}' \\ \dot{v}' \\ \dot{w}' \end{pmatrix} = \begin{pmatrix} f_1(u',v',w',t) \\ f_2(u',v',w',t) \\ f_3(u',v',w',t) \end{pmatrix}$$
$$= \frac{1}{G}S(t)A(t)S^{-1}(t)\begin{pmatrix} u' \\ v' \\ w' \end{pmatrix} - S(t)\begin{pmatrix} \dot{x}_{1nod}(t;R) \\ \dot{x}_{2nod}(t;R) \\ \dot{x}_{3nod}(t;R) \end{pmatrix} \tag{13}$$

and G takes the form $G = u'^2\Phi_1 + u'v'\Phi_2 + v'^2\Phi_3$ with
$\Phi_1 = -\sqrt{\omega_1\omega_2}\cos(\omega_{12}t)\sin 2\phi(t) + \omega_1\sin^2\phi(t)$
$+ \omega_2\cos^2\phi(t)$,
$\Phi_2 = 2\sqrt{\omega_2\omega_3}\cos(\omega_{23}t)\cos\phi(t)\sin\theta(t)$
$- 2\sqrt{\omega_1\omega_3}\cos(\omega_{13}t)\sin\phi(t)\sin\theta(t)$
$+ 2\sqrt{\omega_1\omega_2}\cos(\omega_{12}t)(-\cos\theta(t)\cos^2\phi(t)$
$+ \cos\theta(t)\sin^2\phi(t)) + \cos\theta(t)\sin 2\phi(t)(\omega_1 - \omega_2)$,
$\Phi_3 = -\sqrt{\omega_2\omega_3}\cos(\omega_{23}t)\sin 2\theta(t)\sin\phi(t)$
$- \sqrt{\omega_1\omega_3}\cos(\omega_{13}t)\sin 2\theta(t)\cos\phi(t)$
$+ \sqrt{\omega_1\omega_2}\cos(\omega_{12}t)\cos^2\theta(t)\sin 2\phi(t)$
$+ \omega_1\cos^2\theta\cos^2\phi(t) + \omega_2\cos^2\theta(t)\sin^2\phi(t) + \omega_3\sin^2\theta(t)$.

The equations (13) are subject to the constrain (8) expressed in the new variables (u', v', w'). Thus, only two out of these three variables are independent. Also, up to terms of second order in u'/R or v'/R, the constrain (8) yields $w' = \dot{w}' \simeq 0$. Then the first and second equations of the system (13) approximately become:

$$\begin{pmatrix} \dot{u}' \\ \dot{v}' \end{pmatrix} \simeq \begin{pmatrix} F_1(u',v',t) \\ F_2(u',v',t) \end{pmatrix} = \frac{1}{G}\begin{pmatrix} 0 & B(t) \\ -B(t) & 0 \end{pmatrix}\begin{pmatrix} u' \\ v' \end{pmatrix} - \begin{pmatrix} V_u(t) \\ V_v(t) \end{pmatrix} \tag{14}$$

where $B(t) = -\cos\theta(t)\sqrt{\omega_1\omega_2}\sin(\omega_{12}t)$
$+ \sin\theta(t)\sin\phi(t)\sqrt{\omega_1\omega_3}\sin(\omega_{13}t)$
$- \sin\theta(t)\cos\phi(t)\sqrt{\omega_2\omega_3}\sin(\omega_{23}t)$,

$V_u = \dot{x}'_{1nod} = \sin\phi(t)\dot{x}_{1nod} - \cos\phi(t)\dot{x}_{2nod}$
$V_v = \dot{x}'_{2nod} = \cos\theta(t)\cos\phi(t)\dot{x}_{1nod} + \cos\theta(t)\sin\phi(t)\dot{x}_{2nod}$
$- \sin\theta(t)\dot{x}_{3nod}$

and $\dot{x}_{1nod}, \dot{x}_{2nod}, \dot{x}_{3nod}$ are functions of time found with the help of Eqs.(10).

The key remark is that Eqs.(14) are of the same form as the equations (4) of Ref.[2]. Thus, the analysis of the local structure of the quantum flow of Ref. [2] can be transferred to the present example as well.

In particular: near every nodal point there exists a second type of critical point of the flow, where $\dot{u}' = \dot{v}' = \dot{w}' = 0$. In the approximation of Eqs.(14), we have $w' = 0$, so we can obtain an approximate solution $u' = u'_X, v' = v'_X$ with $F_1(u'_X, v'_X) = F_2(u'_X, v'_X) = 0$, namely

$$\frac{1}{G}B(t)v'_X - V_u(t) = -\frac{1}{G}B(t)u'_X - V_v(t) = 0 \qquad (15)$$

From the above equations we get $v'_X = -\frac{V_u(t)}{V_v(t)}u'_X, u'_X = -\frac{B(t)}{V_v(t)\left(\Phi_1 - \frac{V_u(t)}{V_v(t)}\Phi_2 + \frac{V_u(t)^2}{V_v(t)^2}\Phi_3\right)}$ and $w'_X = 0$. As in [2], we define the Jacobian Matrix at (u'_X, v'_X).

$$J = \begin{pmatrix} \frac{\partial F_1}{\partial u'} & \frac{\partial F_1}{\partial v'} \\ \frac{\partial F_2}{\partial u'} & \frac{\partial F_2}{\partial v'} \end{pmatrix}\Bigg|_{(u'=u'_X, v'=v'_X)} = \begin{pmatrix} a & b \\ c & d \end{pmatrix} \qquad (16)$$

The characteristic polynomial of J

$$\lambda^2 - (a+d)\lambda + ad - bc = 0 \qquad (17)$$

yields two eigenvalues λ_1 and λ_2 which can be proven to be always real and of opposite sign. Consequently the 'X-point' $(u' = u'_X, v' = v'_X)$ is a hyperbolic point.

The denominator G of Eqs. (14) is quadratic in terms of u', v', while their numerator is linear. This implies that the velocity of a trajectory tends to infinity at small distances from the nodal point. We can then approximate locally the trajectory by a so called 'adiabatic approximation'. This means to 'freeze' the time in the right hand side only of Eqs. (14), treating the flow as nearly autonomous for a small time interval around a given t (see [2] for a discussion a the error of this approximation). Then Eqs. (14) take the form

$$\frac{du'}{ds} = F_1(u', v'; t), \quad \frac{dv'}{ds} = F_2(u', v'; t) \qquad (18)$$

where s represents now the time in a small interval around t, while t itself is kept fixed. With the above approximation, Eqs. (18) allow to draw phase portraits yielding the structure of the nodal point-X-point complex. Along the eigendirections corresponding to the eigenvalues of Eq.(17) the (linear) deviations $\Delta u'$ and $\Delta v'$ satisfy the relation $\begin{pmatrix} a & b \\ c & d \end{pmatrix}\begin{pmatrix} \Delta u' \\ \Delta v' \end{pmatrix} = \lambda \begin{pmatrix} \Delta u' \\ \Delta v' \end{pmatrix}$. Hence the eigenvector associated with the eigenvalue λ has a slope $\frac{\Delta v'}{\Delta u'} = \frac{\lambda - a}{b}$. By taking many initial values of $\Delta u', \Delta v'$ (of order 10^{-5}), and integrating (18), we then find the asymptotic curves, i.e. the invariant manifolds from the X-point.

Figure 2 shows an example of nodal point-X-point complex in our model for $t = 4$. The dashed curves show more trajectories of (18) besides the asymptotic curves (red and blue ones). Most of them pass above or below the nodal point X-point complex. Only a few trajectories (those starting between the two blue lines on the left) enter in the region between the nodal point and the X-point. However,

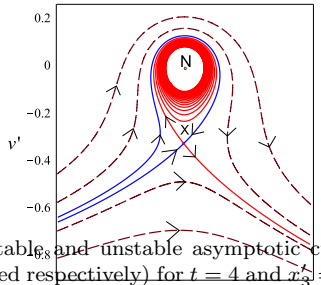

Figure 2: The stable and unstable asymptotic curves from the X-point (blue and red respectively) for $t = 4$ and $x'_3 = 4.23$ (continuous lines). One unstable asymptotic curve spirals around the nodal point and tends to it asymptotically. More trajectories are shown (for other initial conditions) by dashed lines.

the form of the nodal point-Xpoint complex changes with time. In particular, for some times the asymptotic curves that approach the nodal point are stable, while for other times they are unstable. A transition from the first to the second case is shown in Figs 3a-3c. This behavior is characteristic of the local form of the quantum flow after a 'Hopf bifurcation' as discussed in figure (4) of Ref. [2].

Trajectories: We now discuss the behavior of the trajectories near and far from a nodal point-X-point complex.

Figure 4a shows a trajectory (blue) starting at a point close to the nodal point of Fig. 1a and integrated numerically with the exact equations of motion (7) for $t = [1, 100]$. The trajectory drifts on the sphere $R = 4.23$, while it forms several loops on this surface. The moving nodal point on the same surface coincides initially with the guiding center of this motion and remains so up to a time $t \simeq 7.4$. Beyond that time the form of the trajectory changes drastically. The trajectory forms now a box-like motion on the surface of the sphere. Comparing with Fig.1b, we see that the trajectory abandons the neighbourhood of the nodal point when the nodal point accelerates significantly

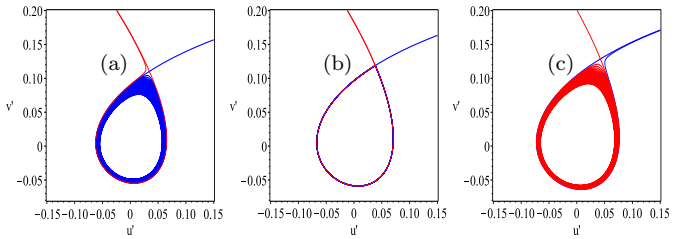

Figure 3: Time evolution of the nodal point-X-point complex around the nodal point at $(x'_3 = 5)$, in a case where the manifold approaching the nodal point from the corresponding X-point turns from stable at $t = 9.52$ (a) to unstable at $t = 9.6$ (c). The transition is made at the time $t = 9.5586$ when the two manifolds coincide around the nodal point (b).

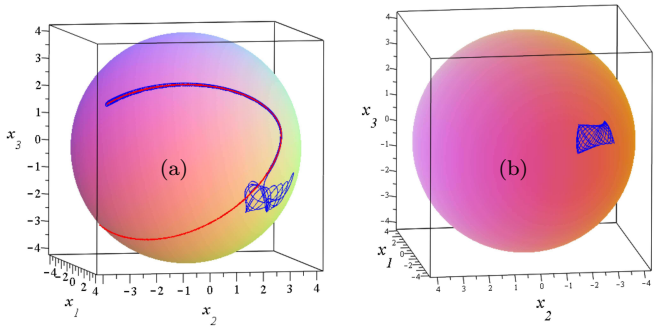

Figure 4: (a) A chaotic Bohmian trajectory starting at a distance 4.23 from $(0,0,0,)$ for $t = 1 \ldots 100$. The trajectory forms a ribbon (blue) around the trajectory of the nodal point (red) up to $t = 7.4$. Then the trajectory deviates from the one of the nodal point and is trapped in a certain region of the same sphere. (b) A trajectory starting away from the nodal lines for $t = 1 \ldots 100$. This trajectory is ordered.

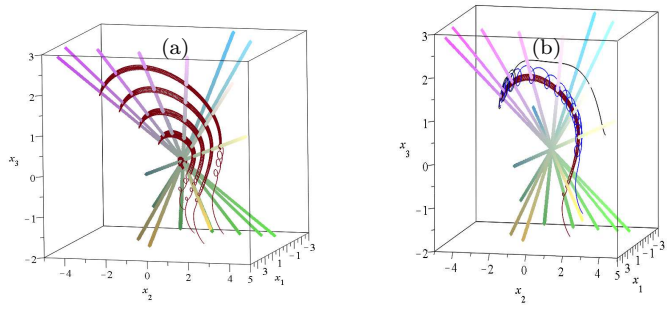

Figure 5: (a) Bohmian trajectories for $t \in [1, 10]$, which start close (at distance $d = 0.1$) to various nodal points at $t = 1$, for different distances R from the origin, namely $R = 0.2, 1.2, 2.2, 3.2$ and 4.2. (b) Bohmian trajectories starting close to the same nodal point but at different distances from it. Namely $d = 0.1$ (crimson), $d = 0.25$ (blue) and $d = 0.3$ (black). Loops around the nodal point disappear faster as d increases.

(Fig. 1b). On the other hand, orbits starting far from the nodal point X-point complex form boxes on the surface of a sphere without exhibiting chaotic behavior (Fig. 4b).

Figure 5a shows five trajectories that start at different distances R from the origin but at the same distance from the corresponding nodal point. All these orbits form loops around the respective nodal points up to a certain time. In fact, as the distance from the origin increases, the time needed for the trajectory to start derailing from the motion of the nodal line decreases. Similarly, Fig. 5b shows three trajectories that start close to the same nodal point but at different distances from it. Then, for a smaller distance from the nodal point we get a longer time for the trajectory to get derailed.

3d nodal point-X-point structures and the emergence of chaos: The nodal point-X-point complexes in our model

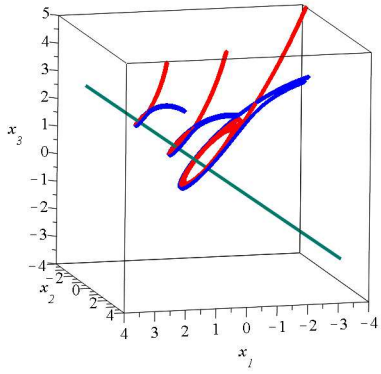

Figure 6: The foliation of nodal point -X-point complexes at $t = 4$ forms a cylindrical structure around the nodal line (green).

are 2-d structures of the quantum flow, parameterized by the radius R of the sphere upon which the considered nodal point moves. However, the foliation of all the planes orthogonal to a nodal line, for different R, forms a 3-d structure containing the union of all nodal point-X-point complexes. This, we hereafter call the '3-d structure of nodal and X-points'. An example of such a 3-d structure is shown in Fig. 6. Along the structure, the complexes are aligned to each other in parallel layers.

The chaotic behavior of trajectories as those given above can now be shown to be due to their scattering by the 3-d structure of nodal and X-points. As an indicator of chaos, we use the Lyapunov Characteristic Number (LCN). Let ξ_k be the length of the deviation vector between two nearby trajectories at the time $t = k\tau,\ k = 1, 2, \ldots$ The stretching number [25] is defined as

$$a_k = \ln\left(\frac{\xi_{k+1}}{\xi_k}\right) \tag{19}$$

and the finite time LCN is given by the equation:

$$\chi = \frac{1}{k\tau}\sum_{i=1}^{k} \ln a_i. \tag{20}$$

The LCN is the limit of χ when $k \to \infty$. Figure 7 shows an example of a trajectory with an abrupt jump of the stretching number at $t \simeq 2$ (red curve). The black curve represents the cumulative stretching number a_{cum} for the same time length, which shows the effect of the jump on the stretching number in the long run. The cumulative value after the end of the event ($t = 6$) is stabilized to a positive value. Furthermore, the distance between the X-point and the trajectory becomes minimum at the time of the jump $t = t_{jump} \simeq 2$. Several such jumps are observed later, and the trajectory eventually stabilizes at a positive value of the LCN, i.e. becomes chaotic. Thus, the scattering by X-points is responsible for chaos in these trajectories.

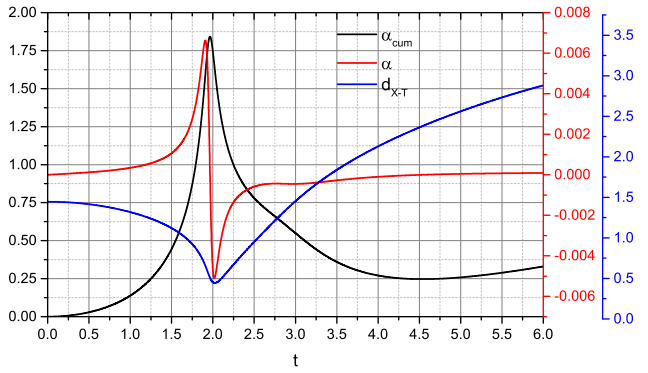

Figure 7: Local chaotic scattering of a trajectory by an X-point (initial conditions $x_1(0) = -1.5, x_2(0) = 2, x_3(0) = -2$). We also compute its deviation vector by numerically solving the variational equations (initial conditions $\delta x_1(0) = 0, \delta x_2(0) = 0, \delta x_3(0) = 1$). The three curves show the value of the stretching number (red), cumulative stretching number (blue) and distance from the X-point (black) as functions of time. All three curves show a sudden jump at $t \simeq 2$, which marks the scattering event. The stretching number is computed with $\tau = 1/100$.

3. Chaotic 3d Diffusion

Our results so far are based on a choice of wavefunction which simplifies both the 3d structure of the nodal point-X-point complexes and the shape of the Bohmian trajectories. Such a choice can serve as the leading approximation for more complex cases, where a small extra term added in the wavefunction leads to a disturbed form of the nodal point-X-point complexes as well as their resulting '3d structure of nodal and X-points'.

As an example, consider the perturbed wavefunction

$$\Psi = a_1\Psi_{1,0,0} + a_2\Psi_{0,1,0} + a_3\Psi_{0,0,1} + a_4\Psi_{0,0,2} \qquad (21)$$

where a_4 is chosen small. We hereafter set $a_1 = 1/\sqrt{3}, a_2 = 1/\sqrt{3}$ and $a_3 = \sqrt{1 - |a_1|^2 - |a_2|^2 - |a_4|^2}$.

An exact computation of the 3-d structure of nodal and X-points using this specific wavefunction (21) is computationally very difficult[1]. Nevertheless, we can assume that for a_4 small, this structure will not be very different from that of the unperturbed case (Fig. 6). In Fig. 8a the latter structure is plotted in the background, along with a chaotic trajectory of (21) for $a_4 = 0.05$. For the perturbed trajectory, the chaotic scattering effects still occur near the X-points. In particular, the trajectory (green curve, for $t \in [0, 100]$) wanders chaotically in the configuration space, its scattering with the '3-d structure of nodal and X-points' taking now place at different distances R from the origin.

[1]Besides the need to find numerically the roots of Eqs. (9) in every time step, in order to compute the X-points, one needs to compute also numerically the foliation of the locally orthogonal surfaces of [23] along the whole nodal line at every time.

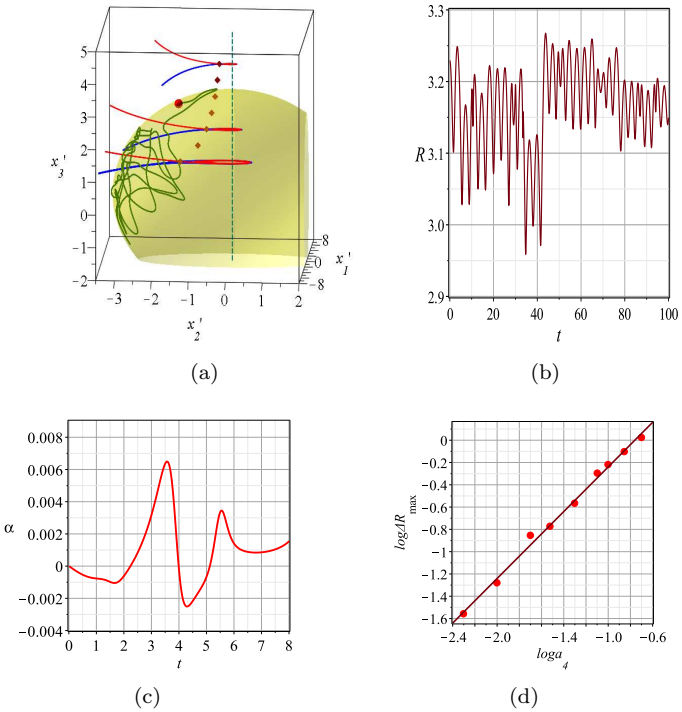

Figure 8: (a) A chaotic Bohmian trajectory (green curve) in the model (21) with $a = 0.05$ and initial conditions $x_1(4) = 2.2194, x_2(4) = -.4062, x_3(4) = 2.3109$. The trajectory is shown in the coordinates (x_1', x_2', x_3') of Eqs. (11). The dashed green line shows the nodal line and the three red-blue curves indicate the manifolds illustrating the corresponding nodal point-X-point structure. The squares indicate the X-line. (b) Variation of the distance $R(t)$ from the origin for the trajectory of (a). (c) A local scattering event (stretching number $a(t)$) around the value $t = 4$ for the same trajectory. The stretching number is computed with $\tau = 1/100$. (d) Dependence of the maximum jump ΔR_{max} in the interval $0 \le t \le 100$ on the perturbation a_4.

The diffusion can be depicted by showing the time variation of the distance R, which now exhibits chaotic variations due to the perturbation $a_4 \neq 0$ (Fig. 8b). Careful inspection reveals that the chaotic variations are correlated with scattering events due to close approach to various X-points of the 3-d structure. In particular, the local jump of the stretching number (Fig. 8c) at a scattering event has a profile quite similar to the one of the unperturbed case (red curve in Fig. 7). Furthermore, we can probe numerically the speed of the chaotic diffusion as a function of the perturbation a_4. Fig. 8d shows how the maximum jump ΔR_{max} of the variation curve of R (as in Fig. 8b) varies with a_4. We find an approximate power law $\Delta R_{max} \sim a_4^p$ in the range $0 < a_4 < 0.2$ with $p \simeq 1$.

4. Conclusions

In this letter we propose a mechanism responsible for the generation of chaos in the Bohmian trajectories of 3-d quantum systems. Our main results are the following:

1. We give numerical (non-schematic) examples of the 3-d structure of the quantum flow close to nodal points delineated along nodal curves, as discussed already theoretically in [23]. To this end, we employ a simple 3-d quantum model described by Eqs.(3-6). When we pass to a moving frame of reference attached to each nodal point, we find that the quantum flow in a surface locally orthogonal to the nodal curve contains a second critical point, whose character is always hyperbolic, thus forming locally a 'nodal point - X-point complex'. Such a complex induces similar topological properties of the quantum flow as those established theoretically in [2] for generic 2-d quantum systems. Also, the union of all the nodal points, along with the X-points and the latter's stable and unstable manifolds, forms a foliation in 3-d space, here called the '3-d structure of nodal and X-points'. This structure complements in an essential way the 'cylindrical structure' of [23], by adding the X-points and their manifolds to it. Here we only give numerical examples of it using a special model. However, we propose the question of how generic this structure is for future study.

2. We give several examples of numerically computed Bohmian trajectories, both ordered and chaotic. The emergence of chaos is connected with the interaction of the trajectories with the 3-d structure of nodal and X-points. In particular, the rise of the Lyapunov exponent is caused by consecutive 'scattering events', taking place whenever a trajectory approaches close to an X-point of the structure. Thus, contrary to the conjecture of [23], chaos is possible even when only one such structure is present in the model.

3. Genuine 3-d chaotic diffusion occurs in models not subject to constraints of the Bohmian trajectories on invariant surfaces (as in Eq. (8)). In general, the approach of a trajectory close to the X-line induces a local drift in the direction *along* the 3-d structure of nodal and X-points. In the example of the model (21) the speed of the drift increases with the parameter a_4, which acts as a perturbation with respect to the model (6) in which no such drift is possible.

Acknowledgements: This research is supported by the Research Committee of the Academy of Athens.

References

References

[1] C. Efthymiopoulos, C. Kalapotharakos, G. Contopoulos, Nodal points and the transition from ordered to chaotic Bohmian trajectories, J. Phys. A 40 (43) (2007) 12945.

[2] C. Efthymiopoulos, C. Kalapotharakos, G. Contopoulos, Origin of chaos near critical points of quantum flow, Phys. Rev. E 79 (2009) 036203.

[3] D. Bohm, A suggested interpretation of the quantum theory in terms of "hidden" variables. i, Phys. Rev. 85 (1952) 166–179.

[4] D. Bohm, A suggested interpretation of the quantum theory in terms of "hidden" variables. ii, Phys. Rev. 85 (1952) 180–193.

[5] P. R. Holland, The quantum theory of motion: an account of the de Broglie-Bohm causal interpretation of quantum mechanics, Cambridge University Press, 1995.

[6] D. Dürr, S. Teufel, Bohmian Mechanics: The Physics and Mathematics of Quantum Theory, Springer, 2009.

[7] A. Benseny, G. Albareda, Á. S. Sanz, J. Mompart, X. Oriols, Applied Bohmian mechanics, Eur.Phys.J. D 68 (10) (2014) 1–42.

[8] X. O. Pladevall, J. Mompart, Applied Bohmian mechanics: From nanoscale systems to cosmology, CRC Press, 2012.

[9] Á. S. Sanz, S. Miret-Artés, A Trajectory Description of Quantum Processes. I. Fundamentals: A Bohmian Perspective, Vol. 850 of LNP, Springer, 2012.

[10] C. Trahan, R. Wyatt, Quantum Dynamics with Trajectories: Introduction to Quantum Hydrodynamics, Interdisciplinary Applied Mathematics, Springer, 2005.

[11] X. Oriols, Quantum-trajectory approach to time-dependent transport in mesoscopic systems with electron-electron interactions, Phys. Rev. Lett. 98 (6) (2007) 066803.

[12] A. Valentini, H. Westman, Dynamical origin of quantum probabilities, in: Proc. R. Soc. A, Vol. 461, 2005, pp. 253–272.

[13] D. Dürr, S. Goldstein, N. Zanghi, Quantum chaos, classical randomness, and Bohmian mechanics, J. Stat. Phys. 68 (1-2) (1992) 259–270.

[14] H. Wu, D. Sprung, Inverse-square potential and the quantum vortex, Phys. Rev. A 49 (6) (1994) 4305.

[15] G. Iacomelli, M. Pettini, Regular and chaotic quantum motions, Phys. Lett. A 212 (1) (1996) 29–38.

[16] H. Frisk, Properties of the trajectories in Bohmian mechanics, Phys. Let. A 227 (3) (1997) 139–142.

[17] D. A. Wisniacki, E. R. Pujals, Motion of vortices implies chaos in Bohmian mechanics, Europhysics Letters 71 (2) (2005) 159.

[18] C. Efthymiopoulos, G. Contopoulos, Chaos in Bohmian quantum mechanics, J. Phys. A 39 (8) (2006) 1819.

[19] D. Wisniacki, E. Pujals, F. Borondo, Vortex dynamics and their interactions in quantum trajectories, Journal of Physics A: Mathematical and Theoretical 40 (48) (2007) 14353.

[20] G. Contopoulos, C. Efthymiopoulos, Ordered and chaotic Bohmian trajectories, Celest. Mech. Dyn. Astron. 102 (1-3) (2008) 219–239.

[21] G. Contopoulos, N. Delis, C. Efthymiopoulos, Order in de Broglie–Bohm quantum mechanics, J. Phys. A 45 (16) (2012) 165301.

[22] I. Bialynicki-Birula, Z. Bialynicka-Birula, C. Śliwa, Motion of vortex lines in quantum mechanics, Phys. Rev. A 61 (3) (2000) 032110.

[23] P. Falsaperla, G. Fonte, On the motion of a single particle near a nodal line in the de broglie–bohm interpretation of quantum mechanics, Phys. Let. A 316 (6) (2003) 382–390.

[24] A. Cesa, J. Martin, W. Struyve, Chaotic Bohmian trajectories for stationary states (2016). `arXiv:1603.01387`.

[25] G. Contopoulos, Order and Chaos in Dynamical Astronomy, Springer, 2002.